Novel laser-processed CsI:Tl detector for SPECT

H. Sabet[a)]
Massachusetts General Hospital, Harvard Medical School, Boston, Massachusetts 02129

L. Bläckberg
Massachusetts General Hospital, Harvard Medical School, Boston, Massachusetts 02129 and Department of Physics and Astronomy, Uppsala University, Uppsala 75120, Sweden

D. Uzun-Ozsahin and G. El-Fakhri
Massachusetts General Hospital, Harvard Medical School, Boston, Massachusetts 02129

(Received 24 July 2015; revised 7 March 2016; accepted for publication 9 April 2016; published 2 May 2016)

Purpose: The aim of this work is to demonstrate the feasibility of a novel technique for fabrication of high spatial resolution CsI:Tl scintillation detectors for single photon emission computed tomography systems.
Methods: The scintillators are fabricated using laser-induced optical barriers technique to create optical microstructures (or optical barriers) inside the CsI:Tl crystal bulk. The laser-processed CsI:Tl crystals are 3, 5, and 10 mm in thickness. In this work, the authors focus on the simplest pattern of optical barriers in that the barriers are created in the crystal bulk to form pixel-like patterns resembling mechanically pixelated scintillators. The monolithic CsI:Tl scintillator samples are fabricated with optical barrier patterns with 1.0×1.0 mm^2 and 0.625×0.625 mm^2 pixels. Experiments were conducted to characterize the fabricated arrays in terms of pixel separation and energy resolution. A 4×4 array of multipixel photon counter was used to collect the scintillation light in all the experiments.
Results: The process yield for fabricating the CsI:Tl arrays is 100% with processing time under 50 min. From the flood maps of the fabricated detectors exposed to 122 keV gammas, peak-to-valley (P/V) ratios of greater than 2.3 are calculated. The P/V values suggest that regardless of the crystal thickness, the pixels can be resolved.
Conclusions: The results suggest that optical barriers can be considered as a robust alternative to mechanically pixelated arrays and can provide high spatial resolution while maintaining the sensitivity in a high-throughput and cost-effective manner. [http://dx.doi.org/10.1118/1.4947294]

Key words: single photon emission computed tomography, laser induced optical barriers, high spatial resolution, CsI:Tl scintillator

1. INTRODUCTION

Molecular imaging of animal models of human diseases has received growing recognition. Visualization of biomarkers and quantification of function in small animal models are challenging and impose stringent requirements on the spatial resolution and sensitivity of the imaging systems. While spatial resolution is critical to realize quantitative high quality images, sensitivity must also be sufficient so that a high quality image can be achieved in a practical acquisition time. Increasing the activity of the injected radiotracer can partially overcome the acquisition time issue; however, it can lead to overexposure to the animal which may alter the physiological parameters in the animal's organs.

Among available imaging modalities, positron emission tomography (PET) and single photon emission computed tomography (SPECT) have received huge attention. Both modalities can provide images with reasonable spatial resolution in a relatively short acquisition time. To show fine details of animal structures, however, the spatial resolution should be further improved. Scintillation detectors have been the mainstay in the majority of the nuclear imaging systems since the introduction of Anger camera.[1] Arrays of photodetectors collect the scintillation photons generated in the scintillation crystals and convert them to electric signal for further processing and image generation. It is well known that the extent of the scintillation light spread grows with the thickness of the scintillator.[2] While some groups have used this feature in monolithic scintillators to derive depth of gamma-ray interaction for PET,[2] large light spread typically results in poor spatial resolution. Therefore in thick scintillators, which are required for high sensitivity detectors, there is typically a pattern of optical structures incorporated into the bulk or surface of a monolithic scintillator.[3,4] The most recognized pattern of optical structures is reflecting materials inserted between individual scintillator elements to form a pixelated scintillator array. Each reflector acts as an optical barrier that reflects the scintillation light and hence confines the light spread resulting in improved spatial resolution. The industry standard to produce such structured scintillators is centered on mechanical pixelation techniques. This process normally involves cutting a monolithic scintillator in one dimension (producing slabs), followed by polishing the slabs and sandwiching them between reflector sheets.[5] The thus formed

block is then cut in the second dimension followed by the polishing and sandwiching process once more. Depending on the scintillation material, this process can be very labor-intensive and cost-prohibitive as the pixel size decreases to sub-mm while the crystal thickness is maintained large enough to provide the required sensitivity. Moreover, due to the need for reflectors, especially in scintillator arrays with small pixel cross section, the packing fraction is low and the sensitivity to incident radiation is poor. Fabrication of small pixel arrays is quite challenging and typically yields in noticeable variation in pixel size which can result in nonuniformity in the detector performance. It should also be noted that mechanical pixelation results in material loss and processing yield issues especially for fabrication of arrays with thick crystals and small pixels.

Other fabrication techniques to provide high spatial resolution scintillators have also been explored. Most notable is thin film scintillator fabrication using physical vapor deposition (PVD),[6,7] which also can be used to force the deposited film to follow a pixelated pattern.[8] In these scintillators, the material is deposited in the form of microcolumns where the size, packing fraction, and thickness of the microcolumns can be controlled by optimizing the deposition parameters. While PVD-based scintillators are attractive to stop low energy x-rays, they are not appropriate for high sensitivity applications since the microcolumn thickness is limited to few hundred microns. Utilizing continuous scintillators, instead of pixelated, has been explored which typically accompanies trading off the sensitivity for better spatial resolution by using rather thin scintillator slabs to compensate for the increased light spread.[9,10]

Semiconductor-based detectors such as cadmium zinc telluride (CZT) and cadmium telluride (CdTe) have received much attention, thanks to their high stopping power and large band gap.[11–13] While CZT and CdTe found their ways in SPECT imaging (such as D-SPECT from Spectrum Dynamics, and Discovery NM-530 from General Electric), increase in readout electronic channels and its associated complexities as the segmentation size becomes smaller leads to unfavorable cost issues.

Thanks to the robust and reliable nature of lasers, pixelating scintillators using laser beams has also been pursued.[14,15] A high intensity laser beam can be used to ablate the scintillator material and create cuts to form pixels. The cut starts from the top surface and the focus of the beam is gradually moved within the crystal to deepen the cut and eventually introduce an all-the-way cut. However, there is an inherent V-shape profile in this pixelation strategy, which can limit the use of this laser ablation technique to thin scintillators.

Recently our group as well as others has utilized an internally focused laser beam to create optical microstructures within the bulk of scintillation crystal.[15–18] It should be noted that, as opposed to the previously mentioned ablation technique, with the internally focused laser beam, the material

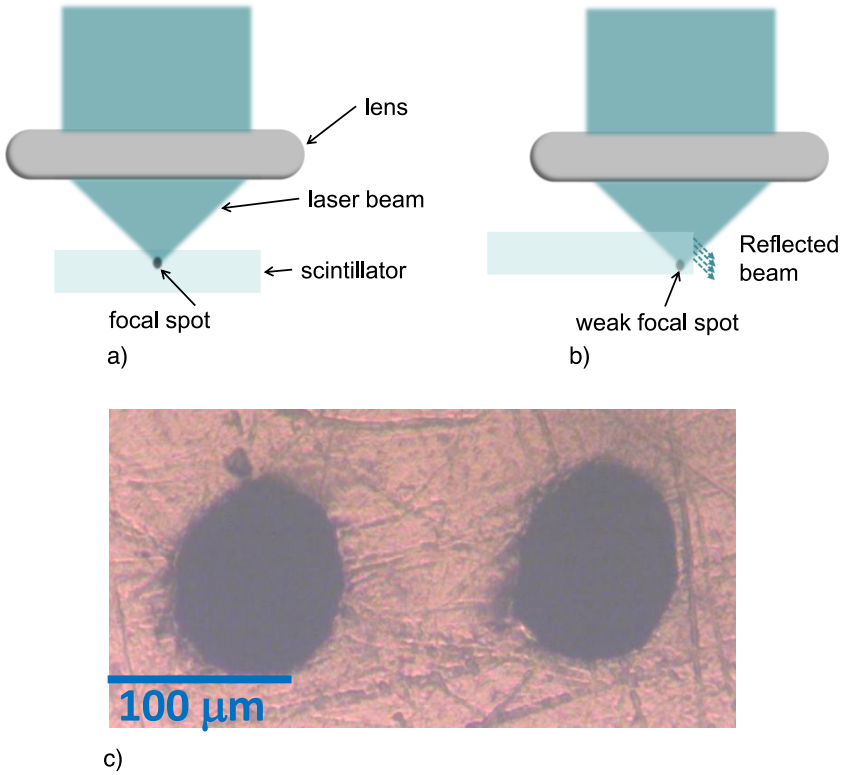

FIG. 1. (a) Schematic drawing of the concept of the LIOB process. Pixelating (or processing) is being performed in the central region of a scintillator where the laser beam is entirely focused within the scintillator bulk. (b) Processing areas near the edge of scintillator showing that part of the beam is placed outside the scintillator volume and therefore the laser beam is partially reflected from the edge surface of the crystal which results in weak focal spot and reduced energy density. (c) A microscopic image of two optical barriers in CsI:Tl with 200 μm spacing. The size of the barriers is 90 ± 7 μm. Note that the scratches seen in (c) are that of the microscope slide as well as typical scratches on crystal surface and not because of the LIOB process.

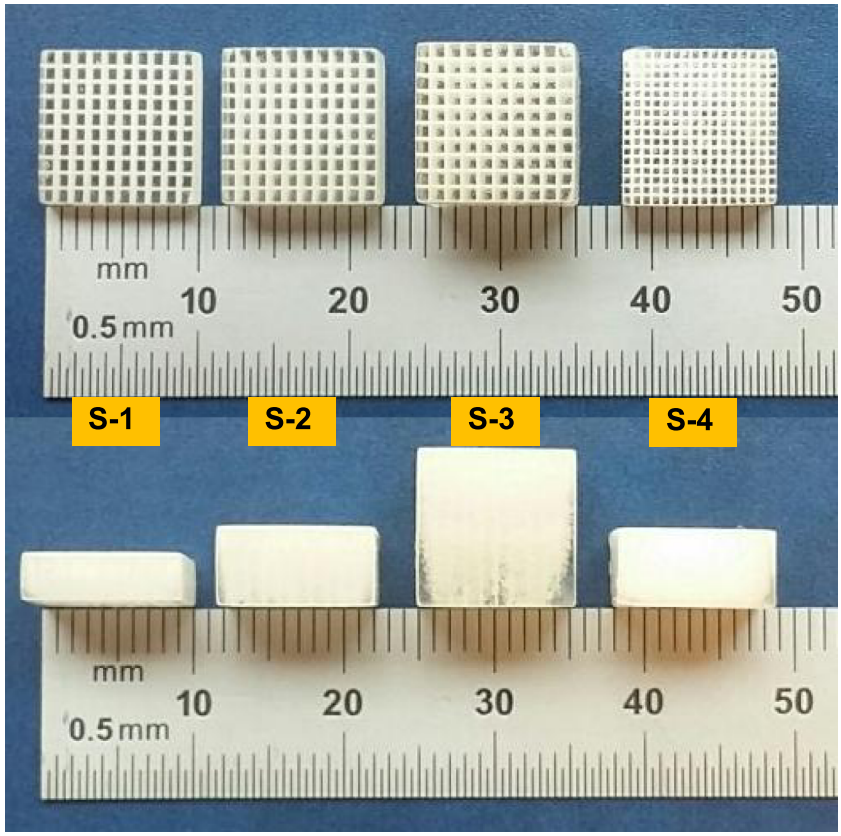

FIG. 2. Photo of the fabricated CsI:Tl arrays processed using the LIOB technique. The arrays measure 10×10 mm^2 in cross section but have different pixel sizes and crystal thicknesses. S-1 to S-3 have 1×1 mm^2 pixels and S-4 has 0.625×0.625 mm^2 pixels (refer to Table I).

is not cut but rather the properties of the material bulk are locally altered. While all the previously reported work are based on utilizing a pulsed laser system with short pulse duration focused inside the scintillation crystal, they differ in the choice of laser system, pulse duration, repetition rate, etc. Furthermore, all the published works are in regard to laser processing of crystals from LSO:Ce scintillator family. Application of these techniques, referred to as laser-induced optical barriers (LIOB) or subsurface laser engraving (SSLE), to scintillators is heavily material dependent in that laser parameters suitable for one material may not work for other materials with different thermal and optical properties. Here we are reporting for the first time, the development of fine-pitched scintillator arrays by employing an optimized LIOB technique for CsI:Tl to realize detectors with sub-mm spatial resolution for SPECT imaging.

2. SCINTILLATOR PROCESSING USING LIOB

The concept of LIOB is shown in Fig. 1(a). A laser beam is focused into the crystal bulk through a lens. Since scintillators are poor thermal conductors, a high intensity laser pulse will generate an excessive heat that cannot be dissipated fast enough, which results in a local damage to the crystal structure. By optimizing the energy and duration of the laser pulse together with the delivery optics, we can control the size of the damaged area and create microstructures with refractive index (RI) different from the surrounding medium. Hereafter we refer to these microstructures as microlenses or optical barriers. According to Fresnel equations, light will be both reflected and refracted at the interface between two media with different RI. Similarly in scintillators processed by the LIOB technique, each optical barrier will reflect and refract the scintillation light. The amount of light reflected by a single optical barrier is a function of its RI with respect to the surrounding medium and the angle of incidence of the light photon. A microscopic image of two optical barriers in a CsI:Tl scintillator is shown in Fig. 1(c). Each barrier is the effect of a single 532 nm laser pulse with ~10 ps pulse duration. The size of the barriers was measured at 90 ± 7 μm with barrier spacing (center-to-center) of 200 μm. By placing such optical barriers throughout the scintillator bulk with optimized barrier density, one can effectively redirect the scintillation light and control its spread and therefore improve the detector spatial resolution. One can imagine that there is a large parameter

TABLE I. Properties of the CsI:Tl crystals pixelated using the LIOB technique.

Sample ID	Crystal dimension (mm^3)	Pixel size (mm^3)	Number of LIOB layers	Pixelation time (min:s)
S-1	$10\times10\times3$	$1\times1\times3$	2	10:49
S-2	$10\times10\times5$	$1\times1\times5$	2	19:10
S-3	$10\times10\times10$	$1\times1\times10$	2	46:21
S-4	$10\times10\times5$	$0.625\times0.625\times5$	2	30:28

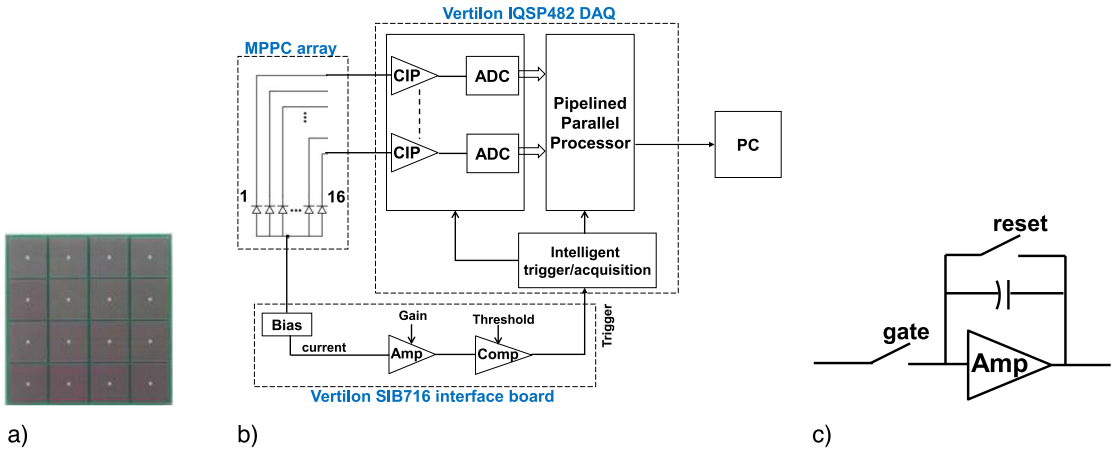

FIG. 3. (a) Photo of TSV-enabled MPPC array used in the experiments. MPPC pixels are 3.0×3.0 mm^2 with a 3.2 mm pitch. Experimental setup used for generating 2D position histograms and line profiles. (b) Schematic drawing of the data acquisition system and the processing electronics. (c) Functional block diagram of the charge integrating amplifier (CIP) used in the Vertilon IQSP482 DAQ. Note that the DAQ, based on a trigger signal from the interface board, closes the gate switch in the CIP amplifier and collects the signal for the length of a user-defined integration window.

space for shape, size, and RI of the optical barriers to be optimized. Furthermore, there might be many barrier patterns with respect to the mentioned parameters that can provide the desired spatial resolution in a given scintillator. As the most basic pattern, optical barriers can be placed side-by-side and along the thickness of the scintillator to create a reflecting wall similar to reflecting materials placed between pixels in mechanically pixelated arrays. For more details on laser processing of scintillators, refer to Refs. 15–17. For simplicity, we refer to the resulting pixel-like shapes as pixel. We would like to emphasize that the LIOB technique is not limited to the creation of traditional pixel-like shapes, but virtually any pattern may be generated within the crystal.

In this work, we fabricated four CsI:Tl crystals using the LIOB technique (see Fig. 2). We used a picosecond laser with 532 nm wavelength. The process was lossless with 100% yield in that after optimizing the laser parameters, we were able to fabricate CsI:Tl detectors with no material waste. Table I shows the pixel size and physical properties of the CsI:Tl crystals. All crystals are 10×10 mm^2 in cross section but with thicknesses ranging from 3 to 10 mm. It should be noted that unlike the distantly placed optical barriers shown in Fig. 1(c), the CsI:Tl detectors in this work are fabricated with overlapping barriers to reduce the interpixel crosstalk.

As described in Refs. 15 and 17, we can control the light response function by a number of techniques such as using single or double pass of laser pulses per optical barrier wall. We define optical wall as the optical structure introduced by the LIOB technique which resembles the reflecting material used in mechanically pixelated arrays. To create an optical wall using a double pass of laser pulses, the laser beam is scanned through the scintillator then jogged by a certain spacing followed by a second pass of laser scanning. While the spacing between the two passes can be any value, we chose 20 μm for the fabricated CsI:Tl arrays reported here. The crystals were mounted on a XYZ linear stage controlled by a software platform with which one can program the stages as well as laser parameters so that the entire process is automated with no human interaction. While the pixel cross section in CsI:Tl arrays S-1 to S-3 is 1×1 mm^2, that of the array S-4 is 0.625×0.625 mm^2. The processing time for each array is also given in Table I. Note that it took only ~30 min to fabricate a

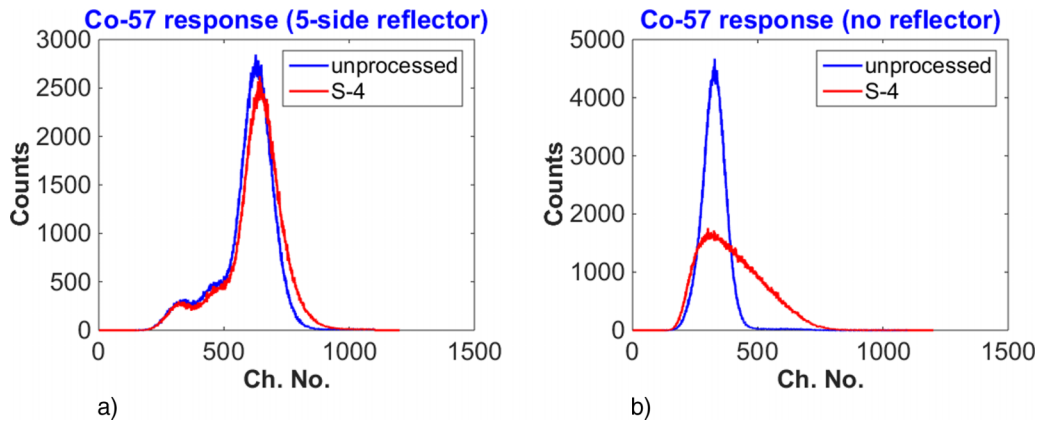

FIG. 4. Co-57 response of S-4 and an unprocessed CsI:Tl crystal in two configurations: wrapped in PTFE in 5-sides (a) and with no reflector (b). The results suggest that the optical barriers do not reduce the light output in CsI:Tl scintillator. When no reflectors applied, there is more collected light at higher energy channels due to light channeling behavior of optical barriers.

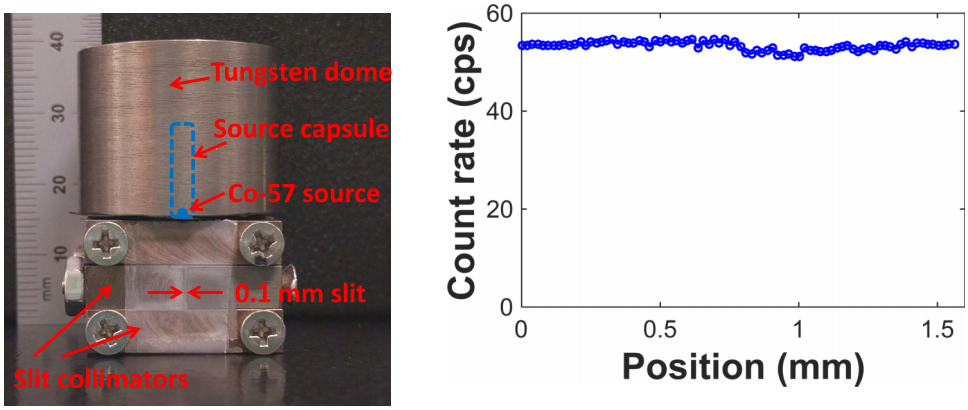

FIG. 5. (a) Photo of collimator with 0.1 mm square hole made up of three 5-mm thick slit collimators. Each slit collimator is built by sandwiching a 0.1 mm thick plastic shim plate between two $20\times10\times5$ mm^3 tungsten slabs. (b) Count rate of three adjacent CsI:Tl pixels of S-4 as a function of the collimated source location. We scanned the source across the three pixels in 20 μm steps crossing two of the optical barrier walls. The recorded data show no noticeable change in the count rate (cps) when crossing the barriers. Therefore we conclude that the optical barriers are still sensitive to the radiation and hence the CsI:Tl detectors fabricated by LIOB have 100% packing fraction.

$10\times10\times5$ mm^3 CsI:Tl detector with 0.625×0.625 mm^2 pixels (256 pixels) without the need for extra steps such as scintillator element polishing and reflector placement that are associated with the mechanical pixelation process. We used a single laser beam in the experiments; however, the processing time can be further reduced by various techniques such as using multiple beams to sub-10 min.

3. DETECTOR EVALUATION

3.A. Readout

We used a Hamamatsu S12642-0404PA-50 multipixel photon counter (MPPC) to read out the light from the fabricated arrays. This device utilizes through silicon via (TSV) that allows for a smaller inter-MPPC pixel dead space of 0.2 mm. A photo of the MPPC along with the experimental setup is shown in Fig. 3. The MPPC pixels are 3×3 mm^2 with 3.2 mm pixel pitch. We used a light diffuser to spread scintillation light over multiple MPPC pixels. This is necessary when using the centroid event positioning algorithm. In this design, we utilized a $14\times14\times1$ mm^3 GE-214 fused silica as light diffuser. It should be noted that the size of the light diffuser is larger than the MPPC device which is helpful for intermodular light sharing between adjacent MPPC arrays.[19] When using the centroid method, the detector resolution normally degrades near the detector edge. Therefore, light sharing between neighboring MPPC arrays can compensate for this resolution degradation. Only the top surface of the fabricated scintillators was covered by 2-layer of PTFE reflector and the sides were left open to allow the light travel to the adjacent MPPC array in our light sharing design concept.

The detectors thus formed were mounted on a Vertilon interface board (SIB716) where all 16 MPPC signals are passed to Vertilon IQSP482, a 64-Ch data acquisition system, for further processing [see Figs. 3(b) and 3(c)]. A charge integrating amplifier (CIP) acting as preamplifier is embedded with each analog to digital converter (ADC) in the DAQ system. A user-selectable threshold in the interface board is used to trigger the IQSP482 after which the DAQ closes the gate switch of the CIP to allow charge integration for a user-specified integration time. Since the trigger signal in IQSP482 is limited to a multiplier of the system reference clock, the charge integration will not be complete resulting in scintillation light loss affecting the energy resolution. While using a DAQ that allows complete light collection would provide better results, in this work we only focus on evaluating the scintillator array fabrication technique and not on the electronic readout. It should be noted that we did not incorporate any temperature compensation technique in the detector housing to correct for the adverse effects of temperature on MPPC performance. However we performed the experiments in air-conditioned experiment room at 22 °C.

3.B. Detector characterization

We first evaluated the effect of optical barriers on light output of the CsI:Tl crystals. We compared S-4 with an unprocessed monolithic CsI:Tl crystal with the same dimensions under two scenarios: three layers of PTFE applied to 5-sides of the crystal, and without reflector. Figure 4 shows the energy spectra of the crystals exposed to a flood Co-57 source. As the results suggest, there is no noticeable change in the light output of the laser-processed CsI:Tl compared with a monolithic crystal when using 5-side reflector. However when there is no reflector applied, there will be larger light collection at higher energy bins since the optical barriers channel the scintillation light.

We also performed an experiment to examine whether the affected areas by LIOB are sensitive to gamma-ray or not. We used a highly collimated Co-57 source using three layers of slit collimator, each with two slabs of 5 mm thick tungsten separated with a 0.1 mm thick plastic shim. The three slit collimators were placed on top of each other where the central collimator was rotated 90°. This configuration realizes a square-hole collimator with 15 mm thickness and 0.1 mm hole size. We scanned the thus formed beam source across

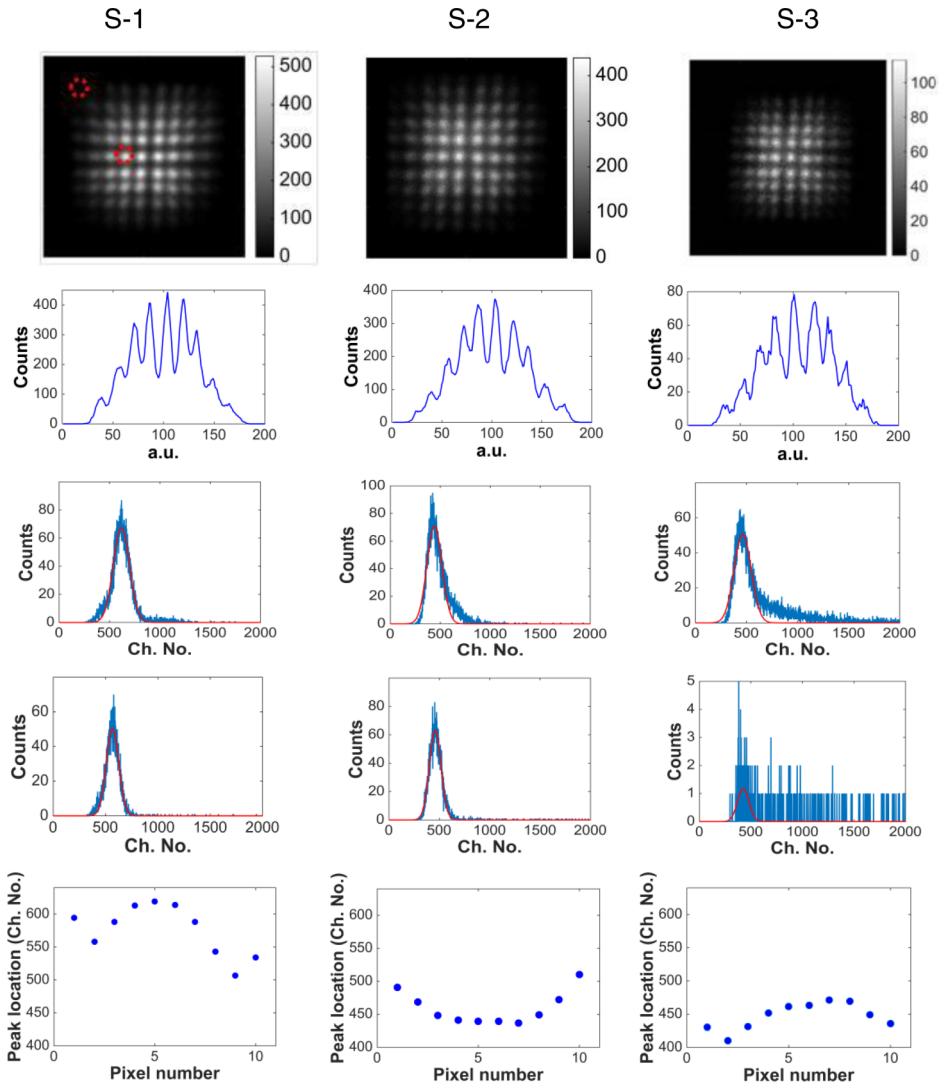

FIG. 6. From top to bottom: flood image, line profile from central column, energy spectra of central and corner pixels, and photopeak location of fabricated CsI:Tl arrays S-1, S-2, and S-3, respectively. The figures were generated by exposing the arrays to 122 keV gamma-rays (Co-57). Note that the arrays have 1×1 mm^2 pixel cross section and thicknesses of 3, 5, and 10 mm from left to right, respectively. For better observation of the flood map, the location of central and corner pixels is shown only in S-1 flood map.

three adjacent pixels of S-4 starting from the central area of one pixel and passing to two barriers until we reached the central area of the third pixel (see Fig. 5). We acquired data for 4 min per step and step size of 20 μm. The recorded data did not show any reduction in the count rate when crossing the optical barriers suggesting that the regions affected by the LIOB process are still sensitive to the gamma-rays and scintillate.

The fabricated scintillators were exposed to a 122-keV gamma-ray source (Co-57) for flood map, pixel separation, and their relative energy resolution evaluation. Figure 6 shows flood maps, line profiles, and energy spectra for central and corner pixels for arrays S-1, S-2, and S-3. Shown is also the photopeak location (channel number) for all pixels in one central CsI:Tl column for each of the arrays. All three arrays have 1×1 mm^2 cross sectional pixel size. It is seen that most of pixel-like elements are well resolved, especially in the center of the maps. However, some of the side pixels show lower count intensity, which is mainly due to the geometry of the experiment, the DAQ, and the light guide size. The larger light guide results in loss of scintillation light when, as in this experiment, only one detector module is used. The effect is more apparent in the edge pixels than the central pixels. As mentioned earlier, the larger light guide is required when coupling multiple detector modules next to each other so that the light generated in a side pixel will be traveling to the neighboring module. The calculated peak-to-valley (P/V) ratios of the arrays are summarized in Table II. The reported P/V values are average of the P/Vs in rows and columns of CsI:Tl in half of the flood images since the maps are symmetric. Two average P/V values are reported, one for all pixels in the

TABLE II. Peak-to-valley ratios for the fabricated CsI:Tl arrays.

	S-1	S-2	S-3	S-4
Total P/V	2.26	2.76	3.05	2.62
Central P/V	2.47	2.69	2.86	2.47

profiles and one for the central pixels in each line profile. For those nonresolved pixels, the P/V was set to 1.0 meaning the pixels are not resolved.

The energy spectra in all arrays show poor energy resolution >25% in the entire detector area, which is mainly due to suboptimal scintillation light collection with the current DAQ system. Furthermore, the location of the photopeak varies between pixels in the same array, suggesting that the light guide thickness can be further optimized, or that the flood map should be corrected for nonuniformity across the detector area.

Figure 7 shows the result for array S-4 as a response to 122 keV gamma-rays. In the flood map and the line profile, nearly all 0.625 mm pixel-like elements are resolved with average P/V of 2.47 and 2.67 in central and entire regions, respectively, suggesting that ~26 CsI:Tl pixels can be resolved per SiPM pixel (3.2 mm pitch). Energy spectra for all 16 pixels along the 8th CsI:Tl column in the flood map are shown in the same figure.

4. DISCUSSION

The results presented in Figs. 6 and 7 suggest that there is no significant change in P/V values when the scintillator thickness is increased. We have shown that 0.625 mm CsI:Tl pixels fabricated with the LIOB technique can be effectively resolved. These results are very encouraging in that now, achieving 0.5 mm pixels for high-spatial resolution SPECT is within reach with low fabrication cost. The time to pixelate this fine-pitched CsI:Tl array was ~30 min with no human interaction, which is fast compared to the labor and processing time associated with mechanical pixelation including polishing, and inserting reflectors between scintillator pixels. With the encouraging result presented in Fig. 5, we believe that these laser-processed CsI:Tl crystals, similar to monolithic crystals, have 100% packing fraction in that the crystal areas affected by laser pulse (i.e., optical barriers) still yield the same sensitivity to radiation.

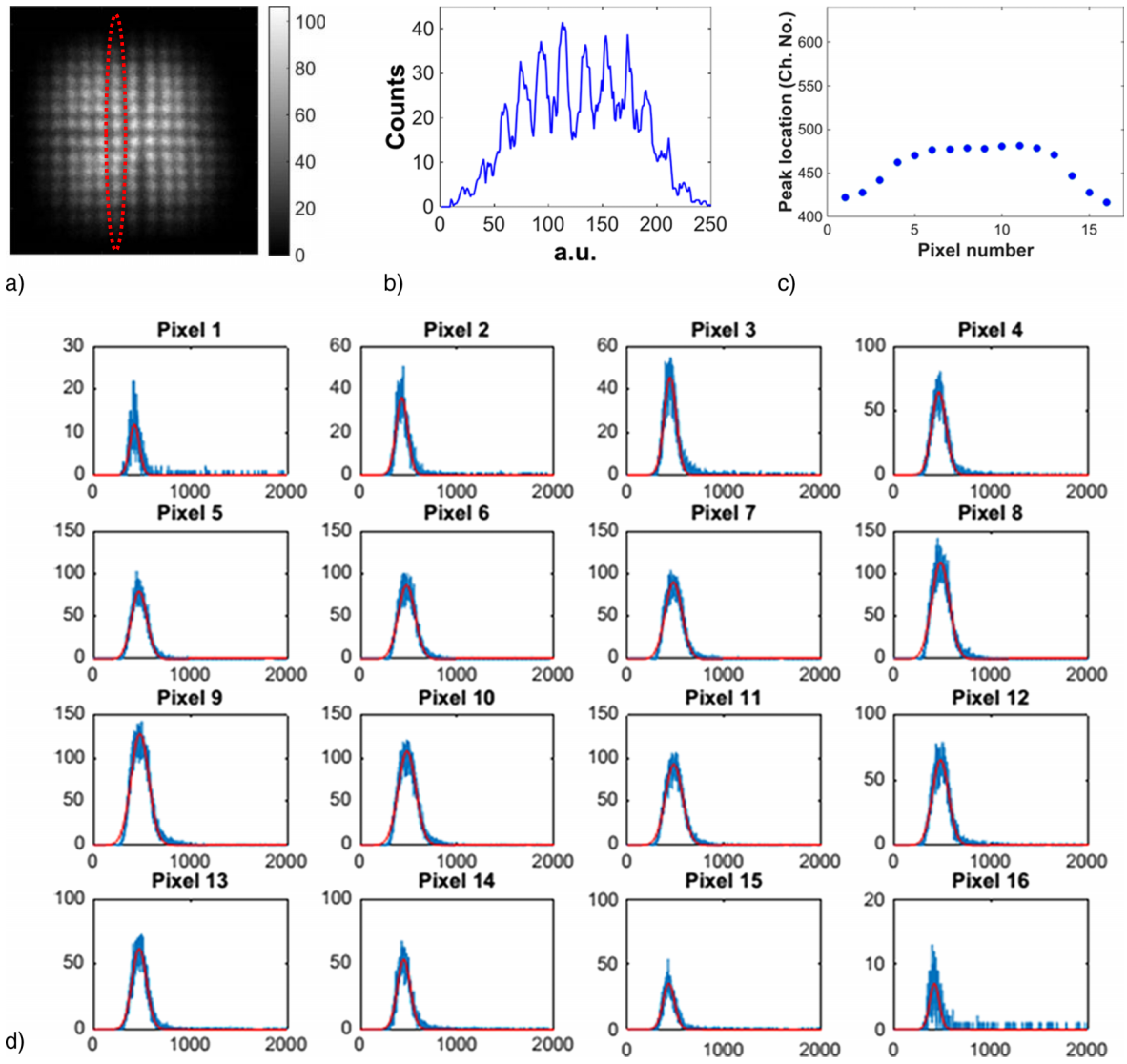

FIG. 7. (a) Flood map, (b) line profile, (c) photopeak locations, and (d) energy spectra for array S-4. This array has $0.625 \times 0.625 \times 5$ mm^3 pixels. In the flood map, nearly all pixels are resolved with P/V value of 2.47 and 2.67 for central and entire detector areas, respectively.

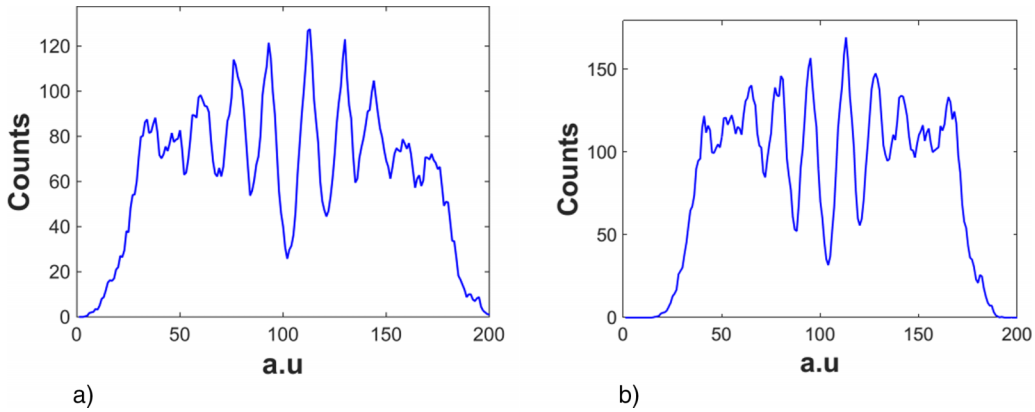

FIG. 8. Beam scan results of S-1 with two reflector configurations: 1-side (top surface) reflector only shown in (a), and 5-sides reflector (top surface with PTFE and side reflectors with ESR film) in (b). The line profiles are drawn through the central row of the scintillator array. With both reflector configurations, all the CsI:Tl pixels are resolved. The average P/V ratio is slightly better when using 5-side reflector (2.8 vs 2.5).

The side pixels are not well resolved especially in array S-3 and S-4. The first reason is due to the laser beam weakening effect close to the edge of the crystal. This effect is illustrated in Fig. 1(b). Part of the laser beam is placed outside the scintillator crystal when processing near the crystal edge. This results in beam reflection from the sides of the crystal which weakens the laser pulse density and hence reduces the reflectivity of the optical barriers. This problem is more pronounced near the edge of thick scintillators. There are many ways to address this issue such as utilizing a lens with longer focal point or placing transparent materials with similar refractive index next to the four sides of the crystal. It should be noted that correcting for this effect was not the focus of this work, and various correcting techniques will be pursued for the future work.

Another reason for the relatively poor performance of the side pixels is scintillation light loss due to the use of $14 \times 14 \times 1$ mm^3 light guide which extends beyond the boundaries of MPPC array. While this affects the performance of the whole array, it is especially pronounced for the pixels close to the side of MPPC array. However, as previously mentioned, this configuration is necessary to let the scintillation light travel to the adjacent modules in order to resolve the side pixels when using centroid event positioning algorithm. Another source of light loss is how the Vertilon DAQ functions which does not allow for full light collection due to the triggering scheme. Furthermore, we speculated that the experiment configuration for generating flood maps (such as close proximity of the flood source to the crystal) might lead to reduced counts for the side and corner pixels. Therefore we performed beam scan for S-1 to further investigate this issue. S-1 was selected due to its smaller thickness compared with other crystals where the beam weakening issue near the crystal edge is less severe in S-1 compared to thicker crystals. It should be noted that by performing a beam scan with the same acquisition time per pixel, most of the geometrical factors will be eliminated. The experiments were carried out for two reflector configurations: (1) PTFE reflector only for top surface and (2) PTFE for top surface and ESR film for other four crystal sides. We fabricated a cylindrical tungsten collimator with 0.5 mm hole diameter and 40 mm hole length. A 5 mCi Co-57 source with 0.75 mm diameter active area was placed behind the hole and aligned with the collimator hole. With both reflector configurations, we were able to identify all 10 pixels in the line profiles (see Fig. 8). As shown in the figures, unlike the results in Figs. 6 and 7, gamma-ray counts for the side pixels are also comparable to that of central pixels. The average P/V ratio for one central row of the pixels is calculated as 2.5 and 2.8 for 1-side and 5-side reflector configurations, respectively.

We used centroid event positioning for generating the flood decoding maps and evaluation of the fabricated arrays. Centroid algorithm and flood decoding maps are typically used with mechanically pixelated scintillators to identify individual scintillator elements as a volume of gamma-ray interaction. However, more sophisticated and accurate event positioning methods have been used in monolithic crystals as well as fine-pitched pixelated arrays where individual elements cannot be identified in the flood maps. The laser-processed scintillators using the LIOB technique should be treated as scintillators whose behaviors are categorized between that of the monolithic and mechanically pixelated crystals. While we showed that by manipulating the laser pulse parameters, we can achieve good pixel separation similar to mechanical pixelated arrays, it is apparent that statistical positioning algorithms such as maximum-likelihood methods can potentially enhance the results.[20]

5. CONCLUSION

We have shown that high spatial resolution and high sensitivity CsI:Tl arrays can be fabricated using the LIOB technique with 100% process yield. In this work, we presented the results of scintillators with built-in optical microstructures that resemble mechanically pixelated scintillator arrays. One should note that with the robustness of LIOB, we can now create any optical pattern within a monolithic scintillator. Therefore the laser-processed scintillators should be seen as a flexible alternative to monolithic and pixelated scintillators that can provide the high sensitivity, low cost, depth of interaction (DOI) information of monolithic crystals, as well as high intrinsic spatial resolution of pixelated scintillators.

Noteworthy that using the LIOB technique does not affect the light output of the CsI:Tl crystals and provide detector arrays with 100% packing fraction in that regions in the crystals affected by laser pulses are still sensitive to the gamma-ray radiation. While DOI in SPECT may not be as critical as in PET, with the flexibility of LIOB we can create patterns similar to a scintillator array with focused-cut elements to avoid DOI blurring when using pinhole collimators.[21] With pinhole collimation and an improved detector intrinsic spatial resolution, one can achieve reduction in multiplexing effect or add more pinholes which results in higher achievable sensitivity. These performance improvements can be achieved while maintaining the detector fabrication cost when using the LIOB technique.

ACKNOWLEDGMENTS

The authors thank Dr. Arkadiusz Sitek for fruitful discussions. Lisa Bläckberg acknowledges support from the Swedish Research Council (VR). This work was supported in part by the U.S. National Institute of Health under Grant Nos. 1R21EB020162-01A1 and 1R03EB020762-01.

[a]Author to whom correspondence should be addressed. Electronic mail: hsabet@mgh.harvard.edu

[1]H. Anger, "Scintillation camera," Rev. Sci. Instrum. **29**, 27–33 (1958).
[2]J. G. Rogers, D. P. Saylor, R. Harrop, X. G. Yao, C. V. M. Leitao, and B. D. and pate, "Design of an efficient position sensitive gamma ray detector for nuclear medicine," Phys. Med. Biol. **31**, 1061–1090 (1986).
[3]J. S. Karp and G. Muehllehner, "Performance of a position-sensitive scintillation detector," Phys. Med. Biol. **30**(7), 643–655 (1985).
[4]M. Kaul, S. Surti, and J. S. Karp, "Combining surface treatments with shallow slots to improve the spatial resolution performance of continuous, thick LYSO detectors for PET," IEEE Trans. Nucl. Sci. **60**, 44–52 (2013).
[5]M. S. Andreaco, C. W. Williams, J. C. Moyers, and K. Vaigneur, "Method for producing a high resolution detector array," U.S. patent, US6749761 B1 (15 June 2004).
[6]V. V. Nagarkar, I. Shestakova, V. Gaysinskiy, S. V. Tipnis, B. Singh, W. Barber, B. Hasegawa, and G. Entine, "A CCD-based detector for SPECT," IEEE Trans. Nucl. Sci. **53**, 54–56 (2006).
[7]H. Sabet, G. Prekas, M. Breen, H. Bhandari, P. Nickerson, G. Derderian, F. Robertson, H. Kudrolli, S. Cool, and V. V. Nagarkar, "A high-perfomance and cost-effective detector using microcolumnar CsI: Tl and SiPM," IEEE Trans. Nucl. Sci. **59**, 1841–1849 (2012).
[8]H. Sabet, H. B. Bhandari, H. Kudrolli, S. R. Miller, and V. V. Nagarkar, "A method for fabricating high spatial resolution scintillator arrays," IEEE Trans. Nucl. Sci. **60**, 1000–1005 (2013).
[9]J. Joung, R. S. Miyaoka, and T. K. Lewellen, "A high resolution animal PET using continuous LSO with a statistics based positioning scheme," Nucl. Instrum. Methods Phys. Res., Sect. A **489**, 584–598 (2002).
[10]D. R. Schaart, H. T. van-Dam, S. Seifert, R. Vinke, P. Dendooven, H. Löhner, and F. J. Beekman, "A novel, SiPM-array-based, monolithic scintillator detector for PET," Phys. Med. Biol. **54**, 3501–3512 (2009).
[11]H. B. Barber, "Applications of semiconductor detectors to nuclear medicine," Nucl. Instrum. Methods Phys. Res., Sect. A **436**, 102–110 (1999).
[12]L. Cai, X. Lai, Z. Shen, C. T. Chen, and L. Meng, "A sub-500 mm resolution MR-compatible SPECT system for simultaneous dual-modality study of small animals," Nucl. Instrum. Methods Phys. Res., Sect. A **734**, 147–151 (2014).
[13]M. Fiechter, J. R. Ghadri, S. M. Kuest, A. P. Pazhenkottil, M. Wolfrum, N. K. Nkoulou, R. Goetti, O. Gaemperli, and P. Kaufmann, "Nuclear myocardial perfusion imaging with a novel cadmium-zink-telluride detector SPECT/CT device: First validation versus invasive coronary angiography," Eur. J. Nucl. Med. Mol. Imaging **38**, 2025–2030 (2011).
[14]V. V. Nagarkar, S. V. Tipnis, K. Shah, I. Shestakova, and S. Cherry, "A high efficiency pixelated detector for small animal PET," IEEE Trans. Nucl. Sci. **51**, 801–804 (2004).
[15]H. Sabet, H. Kudrolli, B. Singh, and V. V. Nagarkar, "Fabricating high resolution and high-sensitivity scintillator arrays using laser induced optical barriers," in *IEEE NSS-MIC Conference Record, Anaheim, CA* (IEEE, New York, NY, 2012), pp. 4080–4084.
[16]T. Moriya, T. Sakai, S. Ohsuka, T. Okamoto, H. Takahashi, M. Watanabe, and T. Yamashita, "Development of PET detectors using monolithic scintillator crystals processed with sub-surface laser engraving technique," IEEE Trans. Nucl. Sci. **57**, 2455–2459 (2010).
[17]H. Sabet and G. El-Fakhri, "Novel, cost-effective, and high-performance modular detectors for emission tomography systems," in *IEEE NSS-MIC, M04-02, Seattle, WA* (2014).
[18]W. C. J. Hunter, R. S. Miyaoka, L. MacDonald, W. McDougald, and T. K. Lewellen, "Light-sharing interface for dMiCE detectors using sub-surface laser engraving," IEEE Trans. Nucl. Sci. **62**, 27–35 (2015).
[19]H. Sabet, H. Liang, Y. Li, and W. Chang, "Development of a modular detector system for C-SPECT," in *IEEE NSS-MIC Conference Record, Knoxville, TN* (IEEE, New York, NY, 2010), pp. 2545–2548.
[20]R. M. Gray and A. Macoviski, "Maximum a posteriori estimation of position in scintillation cameras," IEEE Trans. Nucl. Sci. **23**, 849–852 (1976).
[21]C. H. Baek, H. I. Kim, J. Y. Hwang, S. J. An, K. H. Kim, S. W. Kwak, and Y. H. Chung, "Large-angle pinhole gamma camera with depth-of-interaction detector for contamination monitoring," Nucl. Instrum. Methods Phys. Res., Sect. A **648**, S111–S115 (2011).